Available online at www.sciencedirect.com
ScienceDirect
Geochimica et Cosmochimica Acta 75 (2011) 5879–5891
Geochimica et Cosmochimica Acta
www.elsevier.com/locate/gca

SIMS analyses of silicon and oxygen isotope ratios for quartz from Archean and Paleoproterozoic banded iron formations

Philipp R. Heck [a,b,c,*], Jason M. Huberty [a], Noriko T. Kita [a], Takayuki Ushikubo [a], Reinhard Kozdon [a], John W. Valley [a]

[a] NASA Astrobiology Institute and WiscSIMS, Department of Geoscience, University of Wisconsin, 1215 West Dayton Street, Madison, WI 53706, USA
[b] Chicago Center for Cosmochemistry, The University of Chicago, 5734 South Ellis Avenue, Chicago, IL 60637, USA
[c] Robert A. Pritzker Center for Meteoritics and Polar Studies, Department of Geology, The Field Museum, 1400 South Lake Shore Drive, Chicago, IL 60605, USA

Received 9 June 2010; accepted in revised form 15 July 2011; available online 26 July 2011

Abstract

Banded iron formations (BIFs) are chemical marine sediments dominantly composed of alternating iron-rich (oxide, carbonate, sulfide) and silicon-rich (chert, jasper) layers. Isotope ratios of iron, carbon, and sulfur in BIF iron-bearing minerals are biosignatures that reflect microbial cycling for these elements in BIFs. While much attention has focused on iron, banded iron formations are equally banded silica formations. Thus, silicon isotope ratios for quartz can provide insight on the sources and cycling of silicon in BIFs. BIFs are banded by definition, and microlaminae, or sub-mm banding, are characteristic of many BIFs. *In situ* microanalysis including secondary ion mass spectrometry is well-suited for analyzing such small features. In this study we used a CAMECA IMS-1280 ion microprobe to obtain highly accurate (±0.3‰) and spatially resolved (~10 μm spot size) analyses of silicon and oxygen isotope ratios for quartz from several well known BIFs: Isua, southwest Greenland (~3.8 Ga); Hamersley Group, Western Australia (~2.5 Ga); Transvaal Group, South Africa (~2.5 Ga); and Biwabik Iron Formation, Minnesota, USA (~1.9 Ga). Values of $\delta^{18}O$ range from +7.9‰ to +27.5‰ and include the highest reported $\delta^{18}O$ values for BIF quartz. Values of $\delta^{30}Si$ have a range of ~5‰ from −3.7‰ to +1.2‰ and extend to the lowest $\delta^{30}Si$ values for Precambrian cherts. Isua BIF samples are homogeneous in $\delta^{18}O$ to ±0.3‰ at mm- to cm-scale, but are heterogeneous in $\delta^{30}Si$ up to 3‰, similar to the range in $\delta^{30}Si$ found in BIFs that have not experienced high temperature metamorphism (up to 300 °C). Values of $\delta^{30}Si$ for quartz are homogeneous to ±0.3‰ in individual sub-mm laminae, but vary by up to 3‰ between multiple laminae over mm-to-cm of vertical banding. The scale of exchange for Si in quartz in BIFs is thus limited to the size of microlaminae, or less than ~1 mm. We interpret differences in $\delta^{30}Si$ between microlaminae as preserved from primary deposition. Silicon in BIF quartz is mostly of marine hydrothermal origin ($\delta^{30}Si < -0.5$‰) but silicon from continental weathering ($\delta^{30}Si \sim 1$‰) was an important source as early as 3.8 Ga.

1. INTRODUCTION

Banded iron formations (BIFs) are chemical marine sediments composed of alternating iron-rich (oxide, carbonate, sulfide) and silicon-rich (chert, jasper) layers. BIFs are largely restricted to the Precambrian with the oldest BIFs exposed in supracrustal belts of the North American craton as part of the oldest ~3.8 billion year old (Ga) metasedimentary outcrops at Isua, West Greenland (Moorbath et al., 1973) and Nuvvuagittuq, northern Québec (David et al., 2002, 2009; Cates and Mojzsis, 2007). BIF deposition peaked at ~2.5 Ga including the largest BIFs, the coeval Transvaal Supergroup in South Africa, and Hamersley Group in Western Australia, then abruptly ceased after deposition of

* Corresponding author at: Robert A. Pritzker Center for Meteoritics and Polar Studies, Department of Geology, The Field Museum, 1400 South Lake Shore Drive, Chicago, IL 60605, USA. Tel.: +1 312 665 7655; fax: +1 312 665 7641.
E-mail address: prheck@fieldmuseum.org (P.R. Heck).

0016-7037/$ - see front matter © 2011 Elsevier Ltd. All rights reserved.
doi:10.1016/j.gca.2011.07.023

the correlative 1.9 Ga Biwabik, Gunflint, and other BIFs in the Lake Superior district of Canada and the US.

BIFs have been linked with the rise of oxygen in the atmosphere from 2.4 to 2.2 Ga, which is proposed to have caused deep ocean waters to become fully oxygenated (Holland, 1984). An alternate hypothesis attributes the depletion of deep water Fe^{2+} and Fe^{3+} to increasing concentrations of biogenic H_2S, a reactant that removed Fe^{2+} from the ocean and formed Fe sulfides, lowering the concentration of ferric hydroxides and subsequently halting BIF formation for ~1 billion years (Canfield, 1998). BIFs reappear in the Neoproterozoic from 0.8 to 0.6 Ga during the "Snowball Earth" glaciations (Kirschvink, 1992). Subsequently, chemical conditions of the deep ocean, in particular free oxygen, removed dissolved iron thus thereafter preventing further BIF deposition (e.g., Holland, 1984; Canfield, 2005).

BIFs as chemical sediments provide a unique record of the chemistry of Precambrian ocean waters. Silicon concentrations in ocean water as silicic acid (H_4SiO_4) are thought to be high (60–120 ppm; Siever, 1992; Morris, 1993) close to saturation with respect to amorphous silica due of the absence of silica secreting organisms in the Precambrian (Siever, 1992). Additionally, Fe^{2+} concentrations were high (2–50 ppm; Ewers, 1983; Sumner, 1997; Canfield, 2005) due to very low oxygen and sulfate concentrations in the Paleoproterozoic (e.g., Canfield, 2005). In the absence of oxygen, Fe^{2+} hydrous precipitates could have formed directly, whereas Fe^{3+} hydroxides (ferrihydrite) formed via oxidation of Fe^{2+} by biologic and/or abiologic processes (Lepp and Goldich, 1964; Garrels et al., 1973; Cairns-Smith, 1978; Johnson et al., 2008).

Silicon and iron cycles are coupled during BIF deposition but they may be derived from different sources. The source of iron is generally agreed to be hydrothermal fluids (e.g., Bau et al., 1997), whereas silicon can be derived from hydrothermal fluids, low-temperature weathering of continental crust, or a combination thereof (André et al., 2006; Ding et al., 1996, 2004). Experimental evidence has shown that dissolved silica has an affinity for hydrous surfaces of trivalent metal oxides such as Fe^{3+} hydroxides (Jones and Handreck, 1963). Fischer and Knoll (2009) propose a BIF formation model where silicic acid was adsorbed onto Fe^{3+} hydroxide ($Fe(OH)_3$) precipitates containing organic material that sank to the sea floor. There, bacterial oxidation of organic matter and Fe reduction may have occurred (Lovley et al., 1987), and released some if not all of the adsorbed silicic acid. As envisioned by Fischer and Knoll (2009), a large fraction of the dissolved silicic acid was released back into the ocean, whereas a small fraction precipitated as amorphous silica, and eventually transformed to early diagenetic chert.

The origin of silicon in BIFs can be determined by analyzing silicon isotope ratios in BIF quartz. This assumes minimal silicon isotopic fractionation upon formation of amorphous silica, though the processes controlling silicon isotope fractionation are not yet well understood (Milligan et al., 2004). During the precipitation of SiO_2 from water, values of silica $\delta^{30}Si$ (precipitate) are lower than $\delta^{30}Si$ (dissolved) (Li et al., 1995; Ziegler et al., 2005). Kinetic silicon isotope fractionation is observed during weathering (e.g., Ziegler et al., 2005; Georg et al., 2007b) and precipitation of biogenic silica (e.g., De La Rocha et al., 1997; De La Rocha, 2003; Ding et al., 2005, 2008a,b; Opfergelt et al., 2006, 2008; Beucher et al., 2008; Demarest et al., 2009), which shifts the $\delta^{30}Si$ of the precipitate towards lower and higher values, respectively. Further, adsorption experiments of silica onto clay mineral surfaces demonstrate that ^{28}Si is preferentially incorporated over ^{30}Si in the adsorbed silicic acid (Delstanche et al., 2009).

Low $\delta^{30}Si$ values in BIF quartz (Fig. 1; Gongchangling, Jiang et al., 1993; Isua, André et al., 2006; Pilbara, van den Boorn et al., 2007, 2010; Old Wanderer, Steinhoefel et al., 2009) are consistent with measured values of $\delta^{30}Si$ in silica from modern black-smokers ('hydrothermal', Fig. 1) from −0.4‰ (mantle, Georg et al., 2007a) to −3.1‰ (Mariana Trough hydrothermal vents, Wu et al., 2000). BIF quartz with low $\delta^{30}Si$ values are thus interpreted to reflect a hydrothermal source of silicon (Ding et al., 1996; André et al., 2006; Steinhoefel et al., 2009, 2010; Marin et al., 2010).

In contrast, high $\delta^{30}Si$ values in BIF quartz are consistent with $\delta^{30}Si$ values produced by low-temperature weathering (Ziegler et al., 2005; Georg et al., 2007b; Bern et al., 2010). Positive $\delta^{30}Si$ values for dissolved silicon have been reported from modern river waters (De La Rocha et al., 2000; Ding et al., 2004; Georg et al., 2007b). Precambrian river waters were likely different in $\delta^{30}Si$ than today because of the absence of dissolved ^{30}Si-rich phytoliths and freshwater diatom frustules and higher concentrations of silicic acid. Therefore, the best modern analogs for BIFs that have been analyzed are Icelandic rivers due to the sparse vegetation in the catchment area, where dissolved silica $\delta^{30}Si$ values range from −0.08 to +1.46‰ (Georg et al., 2007b). Van den Boorn et al. (2007) interpret positive $\delta^{30}Si$ values of Archean (Pilbara) cherts as direct seawater precipitates and propose that high $\delta^{30}Si$ Archean seawater resulted from a high-$\delta^{30}Si$ riverine source and the absence of silicon isotope fractionating organisms. Intermediate to low $\delta^{30}Si$ values in BIF quartz are interpreted as a mixture of silicon from hydrothermal and continental sources (van den Boorn et al., 2007, 2010; Steinhoefel et al., 2009, 2010; Marin et al., 2010).

In this study we present correlated *in situ* silicon and oxygen isotope ratios for quartz using secondary ion mass spectrometry (SIMS) at a high spatial resolution (10 μm spot size) for Archean and Paleoproterozoic BIFs. The goals of this study are to document $\delta^{30}Si$ values for quartz within individual quartz laminae and between multiple laminae for individual BIFs, to assess the importance of different sources of silicon during the formation of BIF quartz, and to evaluate whether variability of $\delta^{30}Si$ in BIF quartz is primary or secondary in origin.

2. SAMPLES

In this study we investigated 22 samples from four different BIFs (Table 1): Isua, southwest Greenland (~3.8 Ga); Hamersley Group, Western Australia (~2.5 Ga); Transvaal Group, South Africa (~2.5 Ga); and Biwabik Group, Minnesota (~1.9 Ga). We selected the same samples in which Fe isotopes of magnetite and Fe-carbonates were previ-

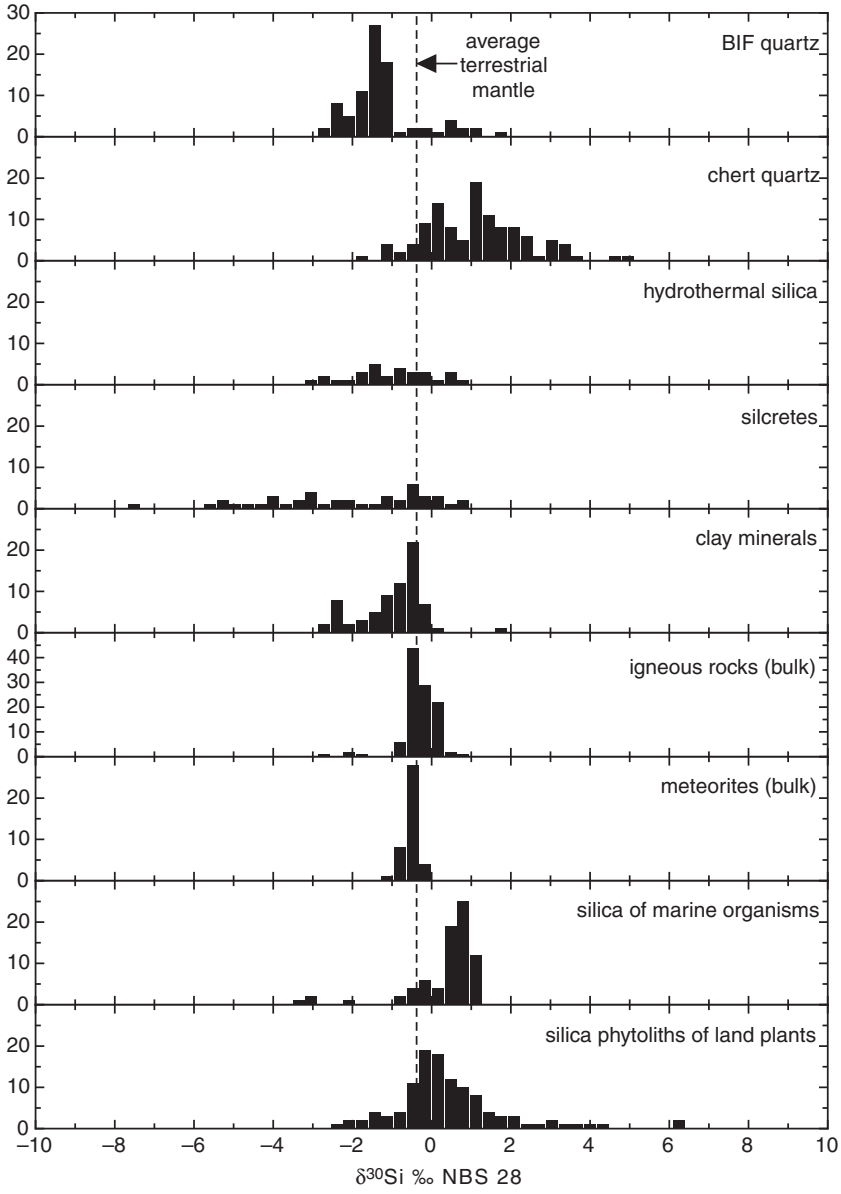

Fig. 1. Histograms of selected published silicon isotope data of representative terrestrial samples and meteorites. Banded iron formations (Jiang et al., 1993; André et al., 2006; Steinhoefel et al., 2009), chert (Douthitt, 1982; Robert and Chaussidon, 2006), hydrothermal silica (Douthitt, 1982; Wu et al., 2000), silcretes (Basile-Doelsch et al., 2005), clay minerals (Douthitt, 1982; Ziegler et al., 2005), bulk igneous rocks (Douthitt, 1982; Ziegler et al., 2005; André et al., 2006; Georg et al., 2007a), bulk meteorites (Molini-Velsko et al., 1986; Georg et al., 2007a), silica of marine organisms (Douthitt, 1982; De La Rocha, 2003; Fripiat et al., 2007; Cardinal et al., 2007) and silica of phytoliths of land plants (Douthitt, 1982; Ding et al., 2005, 2008a; Opfergelt et al., 2008). The average mantle δ^{30}Si value ($-0.38 \pm 0.06‰$; Georg et al., 2007a) is plotted as a vertical dashed line.

ously analyzed by inductively-coupled plasma mass spectrometry at the University of Wisconsin-Madison (Herrick, 2007; Johnson et al., 2003, 2008; Valaas Hyslop et al., 2008) and where the mineralogy has been described (see Table 1; and, e.g., Dymek and Klein, 1988; Klein and Beukes, 1989; Ewers and Morris, 1981; Trendall and Blockley, 1970).

Ten Isua BIF samples of different types were selected for study. Iron isotope ratios for magnetite, iron carbonates, iron silicates, pyrite, and whole-rock samples have been previously determined in these samples (Herrick, 2007). Isua samples are classified as oxide-facies BIFs and are dominantly composed of quartz and magnetite. Two Isua samples contain quartz and large amounts of iron carbonates (is-622-3A and is-711-4A); two other samples contain abundant amphiboles (sm-gr-99-10 and is-625-8C) (Table 1; Dymek and Klein, 1988; Herrick, 2007). Four Hamersley BIF samples are taken from the type-section drill core DDH-47A of the Dales Gorge Member, Brockman Iron Formation, Hamersley Group (Trendall and Blockley, 1970). Hamersley samples are classified as oxide-facies BIFs and are composed of quartz, magnetite, iron carbonates, stilpnomelane, and hematite. One Hamersley sample is a

Table 1
Samples location, ages and most abundant minerals of banded iron formation samples analyzed in this study.

Sample	Abundant minerals	Microanalyses
Isua (Age 3.76 Ga)[1]		
ID-10-2B	Qt, Mt	BSE, SE, CL, $\delta^{30}Si$, $\delta^{18}O$
IS-626-7A	Qt, Mt	BSE, SE, CL, $\delta^{30}Si$, $\delta^{18}O$
IS-629-3B	Qt, Mt	BSE, SE, CL, $\delta^{30}Si$, $\delta^{18}O$
SM-GR-99-21	Qt, Mt	BSE, SE, CL, $\delta^{30}Si$, $\delta^{18}O$
SM-GR-99-4	Qt, Mt	BSE, SE, CL, $\delta^{30}Si$, $\delta^{18}O$
SM-GR-93-42	Qt, Mt	BSE, SE, $\delta^{30}Si$, $\delta^{18}O$
SM-GR-99-10	Qt, Mt	BSE, SE, $\delta^{30}Si$, $\delta^{18}O$
IS-622-3A	Qt, Cb	BSE, SE, $\delta^{30}Si$, $\delta^{18}O$
IS-711-4A	Qt, Cb	BSE, SE, CL, $\delta^{30}Si$, $\delta^{18}O$
IS-625-8C	Qt, Am	BSE, SE, $\delta^{30}Si$, $\delta^{18}O$
Transvaal (Age 2.432 Ga)[2]		
AD-5-aR (152.1 m)	Qt, Cb, Mt	BSE, SE, $\delta^{18}O$
AD-5-bL (152.1 m)	Qt, Cb, Mt	BSE, SE, $\delta^{30}Si$, $\delta^{18}O$
AD-5-cR (152.1 m)	Qt, Cb, Mt	BSE, SE, CL, $\delta^{30}Si$, $\delta^{18}O$
AD-5-dL (152.1 m)	Qt, Cb, Mt	BSE, SE, $\delta^{18}O$
Hamersley (Age 2.780–2.449 Ga)[3]		
2-2C-b (DDH-44, BIF-5, 42.7 m)	Qt, Mt, Cb	BSE, SE, $\delta^{18}O$
3-3A-a2 (DDH-44, BIF-5, 43.9 m)	Qt, Cb, Mt, Ht	BSE, SE, $\delta^{30}Si$, $\delta^{18}O$
3-3A-b (DDH-44, BIF-5, 43.9 m)	Qt, Mt, St	BSE, SE, CL, $\delta^{30}Si$, $\delta^{18}O$
18-2A-b (DDH-44, BIF-13, 103.6 m)	Mt, Qt, Cb	BSE, SE, $\delta^{30}Si$, $\delta^{18}O$
Biwabik (Age 1.8783 Ga)[4]		
03-BIW-35E	St, Qt, Mt, Cb	BSE, SE, CL, $\delta^{30}Si$, $\delta^{18}O$
03-BIW-36 M	Cb, Mt, Qt, St	BSE, SE, CL, $\delta^{30}Si$, $\delta^{18}O$
03-BIW-43B	Mt, Am, Qt	BSE, SE, $\delta^{18}O$
03-BIW-18C	Mt, Qt, Am	BSE, SE, $\delta^{18}O$

Qt = quartz; Mt = magnetite; Cb = carbonate; Am = amphibole; Ht = hematite; St = stilpnomelane. BSE = backscattered electron imaging with the scanning electron microscope (SEM); SE = secondary electron imaging with SEM; CL = cathodoluminescence imaging with SEM. $\delta^{30}Si$ = Si isotope analyses with ion microprobe; $\delta^{18}O$ = oxygen isotope analyses with ion microprobe. Age references: [1]Moorbath et al., 1973; [2]Trendall et al., 1990; 2.521 Ga, Sumner and Bowring, 1996; [3]Trendall et al., 2004; [4]Fralick et al., 2002.

carbonate-rich mesoband composed of ankerite, siderite, quartz, stilpnomelane, and magnetite (2-2C-b, Table 1). Four Transvaal Group BIF samples are taken from drill core AD-5 of the Transvaal Iron Formation (Klein and Beukes, 1989; Beukes et al., 1990; Kaufmann, 1996; Johnson et al., 2003). Transvaal samples are composed of quartz, iron carbonates, and magnetite. Four Biwabik BIF samples, two low-temperature metamorphic grade (~240 °C) and two high-temperature contact-metamorphic grade (~675 °C) were selected for study (Valaas Hyslop et al., 2008). Low-temperature Biwabik samples contain quartz, magnetite, iron carbonates, and stilpnomelane. High-temperature Biwabik samples contain clinopyroxene and olivine in addition to quartz and magnetite (Table 1).

3. METHODS

3.1. Sample preparation

3.1.1. Epoxy mounts

Millimeter to centimeter-sized rock chips were cut from drill core and hand samples with a water-cooled diamond saw, cleaned with distilled water and embedded near the center of 25 mm diameter epoxy plugs. After curing the epoxy mount two days at ~60 °C, the samples were ground with a 6 μm diamond lapping film. After a flat surface was obtained, small <2 mm holes were drilled within 5 mm of the sample center to accommodate a quartz standard (UWQ-1, Kelly et al., 2007). The holes were filled with epoxy and after curing at ~60 °C for two days, the resulting epoxy protuberances were brought to level with the sample surface with a 6 μm diamond lapping film. The sample mount was then polished stepwise with 6, 3, and 1 μm diamond paste. Because our protocol for high precision SIMS analysis requires a smooth, flat sample surface with relief less than a few μm (Kita et al., 2009) sample topography was measured with a ZYGO white light profilometer after polishing and before SIMS analysis.

3.1.2. Thin sections

Preexisting thin sections of four Isua samples (SM-GR-99-10, SM-GR-93-42, IS-625-8C, IS-622-3A; Dymek and Klein, 1988) were cut to 25 mm diameter and used in this study. Subsequently, UWQ-1 standard was face-mounted into the center of each section and they were repolished as described in the previous section.

3.2. Scanning electron microscopy

Prior to SIMS analyses, all samples were carbon coated and imaged with a Hitachi S-3400 N scanning electron microscope (SEM) in backscattered electron (BSE) and

secondary electron (SE) modes. An accelerating voltage of 15 kV and a working distance of ~10 mm were used. After SIMS analyses, all SIMS pits and surrounding areas were imaged in BSE, SE, and for selected spots also in CL mode to determine the accuracy in placement of the ion beam. Data from pits containing a mixture of minerals, large cracks, or large cavities were rejected.

3.3. Secondary ion mass spectrometry

High-precision oxygen- and silicon-isotope analyses were performed with a CAMECA IMS-1280 Ion Microprobe at the WiscSIMS Laboratory at the University of Wisconsin-Madison. Sampling spots were selected based on detailed SEM imaging of all samples. Quartz surfaces free of visible defects and large enough to accommodate the ion beam spot size were selected for analysis. All analysis spots were placed within a radius of 5 mm from the center of the mount. This keeps any XY effect on analytical bias below the reproducibility of the standard as shown by Kita et al. (2009).

3.3.1. Oxygen isotopes

Analytical conditions and procedures for high-precision O-isotope analyses with the IMS-1280 are described in detail elsewhere (Kelly et al., 2007; Kita et al., 2009; Valley and Kita, 2009). We used the same parameters as Kita et al. (2009) and applied a ~2–2.5 nA primary Cs^+ beam focused to a spot size of ~10 × 15 μm. The resulting analysis pit depth is on the order of a micrometer (Kita et al., 2009). A normal-incidence, equal potential electron beam was used for charge compensation. We set and align the electron gun in every session. We did not observe any sign of charging of the samples during the analyses sessions reported in this paper. Secondary ions of $^{16}O^-$ and $^{18}O^-$ were detected simultaneously with two faraday cup (FC) detectors, L1 (10^{10} Ω resistor) and H1 (10^{11} Ω), respectively. Count rates for ^{16}O were ~2.5–3.5 × 10^9 cps (~1.3 × 10^9 cps/nA). Mass resolving power (MRP) was 2200 at 10% peak height. The detectors were realigned to the center of the respective mass peaks every 12 h and the magnetic field was stabilized by NMR probe. Four analyses of the UWQ-1 quartz standard (Kelly et al., 2007) were made before and after each group of 10–20 sample analyses of quartz. The spot-to-spot reproducibility of each group of eight to ten bracketing standard analyses averages ±0.3‰ (2 SD) and the standard error is ±0.1‰ (2 SE).

3.3.2. Silicon

Nearly identical analytical conditions as for oxygen isotope analyses were applied for silicon isotope analyses of quartz. The rationale for the choice of the analytical conditions for silicon isotopes is described in Knight et al. (2009), in which three isotopes of silicon were analyzed. The conditions outlined in Knight et al. (2009) were modified for silicon two-isotope ratios ($^{30}Si/^{28}Si$) to accommodate the requirements of the present study. A primary Cs^+ beam current of ~2.5–3 nA was used to provide $^{28}Si^-$ count rates of ~1 to 1.5 × 10^8 cps (~5 × 10^7 cps/nA). Secondary ions of $^{28}Si^-$ and $^{30}Si^-$ were detected with two FC detectors (with 10^{11} Ω resistors), either with two movable detectors L′2 and H1, or with a combination of movable detector L′2 and the axial detector FC2. We obtain a mass resolving power (MRP, defined as M/ΔM at 10% peak height) of 2200 which is equivalent to a relative mass difference of 455 ppm (ΔM/M). Although ΔM is larger than the difference of mass between ^{30}Si and $^{29}Si^1H$ [ΔM(^{30}Si–^{29}SiH)/M(^{30}Si) = 352 ppm], the $^{29}Si^1H$ hydride peak is outside of the 10% level, which is at ~230 ppm at each side of the center of the ^{30}Si mass spectrum. Therefore, the overlapping tail of the ^{29}SiH peak should have an insignificant affect on the ^{30}Si peak height and shape. The flatness of the plateau of the ^{30}Si mass spectrum lets us quantify the contribution of the ^{29}SiH tail to ^{30}Si, which is less than 0.01‰. There is no sign of a peak height increase towards the higher mass side.

Four analyses of the UWQ-1 quartz standard (Kelly et al., 2007) were made before and after each group of 10–20 sample analyses. The spot-to-spot reproducibility of each group of eight to ten bracketing standard analyses averages ±0.3‰ (2 SD) and the standard error is ±0.1‰ (2 SE).

3.3.3. Standards

The analytical conditions were tested on NBS-28 (also called African Sand and NIST RM 8546) and UWQ-1 quartz standard grains. Oxygen isotope ratios are reported in standard delta notation (δ) in units of per mil (‰) relative to the international reference Vienna Standard Mean Ocean Water (VSMOW), and silicon isotope ratios are reported relative to the NBS-28 quartz standard:

$$\delta^{18}O = 1000 \times \left(\left(\left[{}^{18}O/{}^{16}O \right]_{sample} - \left[{}^{18}O/{}^{16}O \right]_{VSMOW} \right) / \left[{}^{18}O/{}^{16}O \right]_{VSMOW} \right), \quad (1)$$

$$\delta^{30}Si = 1000 \times \left(\left(\left[{}^{30}Si/{}^{28}Si \right]_{sample} - \left[{}^{30}Si/{}^{28}Si \right]_{NBS\text{-}28} \right) / \left[{}^{30}Si/{}^{28}Si \right]_{NBS\text{-}28} \right). \quad (2)$$

This notation is followed throughout this study.

UWQ-1 standard was calibrated by laser-assisted fluorination for oxygen isotopes ($\delta^{18}O = 12.33 \pm 0.14$‰ 2 SD VSMOW, ±0.02 2 SE, $N = 20$, Kelly et al., 2007) and by ICP-MS for silicon isotopes ($\delta^{30}Si = -0.03 \pm 0.08$‰ 2 SD NBS-28, Georg, 2006). Multiple grains of NBS-28 and UWQ-1 were cast in epoxy, polished, and imaged by SEM in BSE and SE modes. These grains were analyzed by IMS-1280 with the same conditions as samples. Secondary ion intensity of ^{28}Si did not change more than a few%. A grain-to-grain $\delta^{30}Si$ (IMF-corrected values using bracketing standards) reproducibility of ±0.2‰ (2 SD, $n = 14$) was obtained on UWQ-1 and of 0.3‰ (2 SD, $n = 26$) on NBS-28 in two analysis sessions separated by 9 months (Fig. 2 and Electronic Annex). These values are similar to the typical external precision of 0.25‰, defined by the 2 SD of a single UWQ-1 standard grain used as the bracketing standard. We use the calibrated quartz standard UWQ-1 to correct our data for instrumental bias for both $\delta^{18}O$ and $\delta^{30}Si$. As a check for internal consistency, the UWQ-1 $\delta^{30}Si$ values were

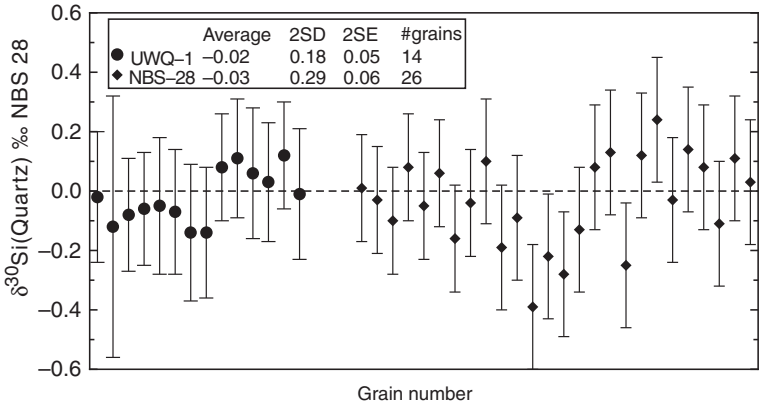

Fig. 2. Ion microprobe measurements of δ^{30}Si (‰ NBS-28) on a polished epoxy mount of UWQ-1 and NBS-28 quartz standard grains. Each data point represents the average of two analyses measured nine months apart. Error bars are ±2 standard deviations. Georg (2006) measured δ^{30}Si of UWQ-1 (-0.03 ± 0.04‰ NBS-28) by ICP-MS. Within uncertainty values of δ^{30}Si of UWQ-1 and NBS-28 are identical. Note, however that homogeneity is better for UWQ-1, which was homogenized during granulite metamorphism, than for NBS-28, which is a sandstone and hence a mechanical mixture from many protoliths (see text). The full data set is reported in the Electronic annex.

determined by 137 SIMS analyses of 14 UWQ-1 grains measured against individual UWQ-1 grains chosen as a running standard (δ^{30}Si(UWQ-1) average = -0.02 ± 0.18‰ NBS-28 2 SD, ±0.05‰ 2 SE, 14 grains). These UWQ-1 values are identical to NBS-28 (53 analyses of 26 grains) measured against the same UWQ-1 grains as a running standard (δ^{30}Si(NBS-28)=-0.03 ± 0.29‰ NBS-28 2 SD, ±0.06 2 SE, 26 grains) and consistent with the calibrated ICP-MS values (Georg, 2006) for NBS-28 (Fig. 2). These average measured values are not statistically different from 0‰. However, there is a 0.11‰ difference in analytical reproducibility defined as 2 SD and shown in Fig. 2. It is not surprising that NBS-28 is slightly heterogeneous from grain-to-grain. This sample is a quartz arenite sandstone and likely contains detrital quartz grains from many protoliths. In contrast, UWQ-1 recrystallized during granulite facies metamorphism and silicon and oxygen isotopes were equilibrated at the scale of the 1 kg sample. The full standard data set is given in the Electronic annex.

Two to three grains of UWQ-1 quartz standard were face-mounted and polished in the center of all sample mounts and used as a bracketing standard.

4. RESULTS

We present 476 analyses of δ^{18}O and δ^{30}Si for quartz bracketed by 477 UWQ-1 standard analyses (Electronic annex). The high proportion of standard to sample analyses and the standard-sample-standard bracketing protocol employed in this study are important for attaining and verifying the high quality of SIMS data.

4.1. Oxygen isotopes in quartz

SIMS analyses of δ^{18}O for BIF quartz (22 samples, $N = 251$) are shown in Fig. 3. Values of δ^{18}O vary from 8.3‰ for Isua to 27.5‰ for a low-temperature Biwabik sample. The average δ^{18}O value is 13.3‰ for Isua, 20.3‰ for low-temperature Biwabik, 15.1‰ for high-temperature Biwabik, 22.4‰ for Hamersley and 22.5‰ for Transvaal. The range in δ^{18}O values is 10.1‰ for Isua, 9.6‰ for low-temperature Biwabik samples, 0.6‰ for high-temperature Biwabik, 4.5‰ for Transvaal, and 4.6‰ for Hamersley. The lowest δ^{18}O values are found in Isua samples ID-10-2B, IS-711-4A and in four analyses of Biwabik low-temperature sample 03-BIW-36M. The highest values of δ^{18}O (>24‰) are found in thin crosscutting quartz veins in a Transvaal sample (see Electronic appendix), however, these are not representative of the BIF sample even on the small scale where we analyze it. Therefore, we do not further discuss data obtained from the rare veins. Besides that, the highest values are observed in three analyses of Biwabik low-temperature sample 03-BIW-35E, one analysis in Hamersley sample 2-2C-b, and two analyses in Hamersley sample 3-3A-b. For the two low-temperature Biwabik samples, the average δ^{18}O value and range in δ^{18}O are calculated excluding high and low analyses (26.2‰, 26.5‰, 26.6‰, 27.5‰ for 03-BIW-35E, and 7.9‰, 8.9‰, and 13.8($n = 2$)‰ for 03-BIW-36M) that are of small domains targeted by ion microprobe not representative of the bulk composition (18.8‰ for 03-BIW-35E and 18.9‰ for 03-BIW-36M; Valaas Hyslop et al., 2008).

4.2. Silicon isotopes in quartz

SIMS analyses of δ^{30}Si for BIF quartz (18 samples, $N = 225$) are shown in Fig. 4. Values of δ^{30}Si display a range of ~5‰ from −3.7‰ in Isua (BIF SM-GR-93-42) to 1.2‰ in Hamersley (BIF 2-2C-B). Aside from a few analyses of quartz overgrowths in silcretes from Cretaceous marine sandstones in southeast France (Fig. 1, δ^{30}Si to −7.5‰; Basile-Doelsch et al., 2005), these are the lowest values in terrestrial samples reported to date. The average δ^{30}Si value for Isua is −1.6‰ while for Hamersley, Transvaal, and Biwabik, the average δ^{30}Si value is identical, -0.6‰. The range in δ^{30}Si values is 4.5‰ for Isua, 3.5‰ for Hamersley, 2.7‰ for Biwabik, and 2.6‰ for Transvaal. The lowest δ^{30}Si value for Isua (−3.7‰) is 1‰ lower and

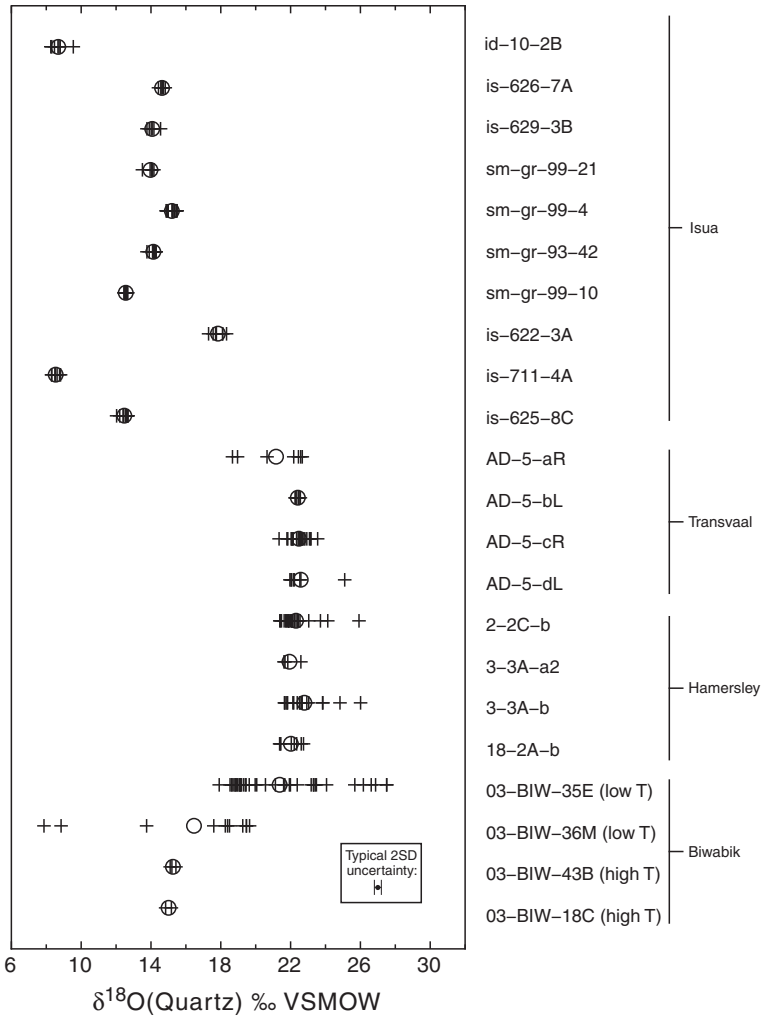

Fig. 3. Oxygen isotope ratios of quartz in banded iron formation analyzed by ion microprobe in this study (crosses = individual analyses; circles = averages). The typical analytical uncertainty is smaller than data points (0.3‰ 2 SD, inset).

the range in δ^{30}Si values is 1‰ greater than for Hamersley, Transvaal and Biwabik.

Variability in δ^{30}Si values is correlated with the scale of analysis for individual BIF samples. Values of δ^{30}Si are heterogeneous by from 1‰ to 3‰ for most samples (Fig. 4). BIF samples with a range in δ^{30}Si of 1–3‰ were analyzed from multiple laminae over mm-to-cm of vertical banding, while samples that are homogeneous in δ^{30}Si were analyzed from an individual sub-mm thick lamina only. BIF samples that vary in δ^{30}Si between multiple laminae are homogeneous for multiple analyses within a single lamina.

5. DISCUSSION

5.1. Distribution of isotope ratios

Oxygen isotope ratios for quartz from Isua are homogeneous within individual samples but are variable from sample-to-sample (Fig. 5). The first order effect of metamorphism is recrystallization, exchange with oxygen-rich/silicon-poor fluids, and faster diffusion at higher temperature, which tend to homogenize isotope compositions and cause inter-mineral exchange at m- to cm-scales. Metamorphic homogenization of oxygen isotopes in quartz at Isua is reflected in the narrow range of δ^{18}O values. Exchange with other minerals, principally magnetite, accounts for lower δ^{18}O values from Isua (~450–600 °C; Dymek and Klein, 1988) and high-temperature Biwabik samples (640 and 700 °C; Valaas Hyslop et al., 2008). This is a result of both recrystallization during prograde metamorphism and diffusion during cooling (e.g., Valley, 2001; Valaas Hyslop et al., 2008). The highest δ^{18}O values and largest range in δ^{18}O are found in Transvaal, Hamersley, and low-temperature Biwabik samples that experienced greenschist facies conditions (max. $T = 300$ C) (Figs. 3 and 5).

In contrast to oxygen isotopes, silicon isotope ratios are heterogeneous by up to 3‰ in Isua samples, similar to the range of 2‰ found in BIFs that have not experienced high temperature metamorphism (up to 300 °C). Fig. 6 shows that values of δ^{30}Si for quartz are homogeneous to ±0.3‰ in individual sub-mm laminae, but vary significantly between multiple laminae over mm-to-cm of vertical banding.

We interpret variability in δ^{30}Si values at Isua to indicate that silicon isotope ratios are preserved from primary

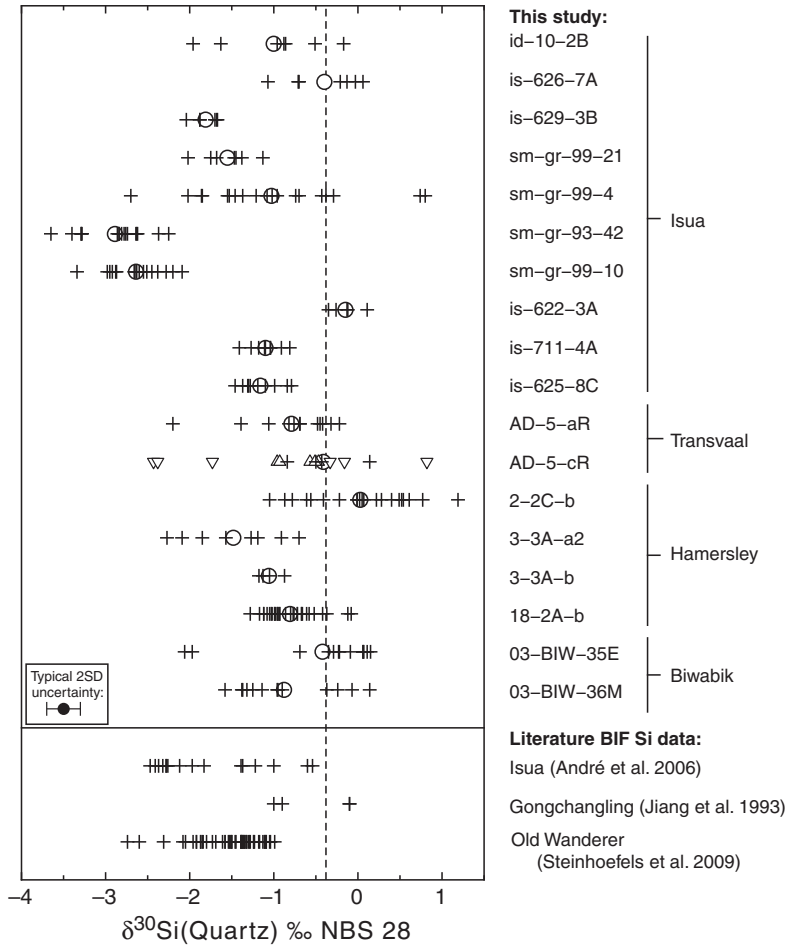

Fig. 4. Silicon isotope ratios of quartz in banded iron formation samples analyzed by ion microprobe in this study (crosses = individual analyses; circles = averages). Also plotted are published values of single $\delta^{30}Si$ analyses that were obtained with different analytical methods: fluorination (Jiang et al., 1993) and laser inductively coupled mass spectrometry (André et al., 2006; Steinhoefel et al., 2009). The typical analytical uncertainty in our study is ±0.3‰ (2 SD, inset). The vertical dashed line is the average terrestrial mantle $\delta^{30}Si$ value (−0.38‰, Georg et al., 2007a).

depositional values and are not homogenized at the cm-scale by amphibolite facies metamorphism. This does not rule out the possibility that metamorphism locally altered silicon isotope ratios of some samples at a smaller scale, such exchange has not occurred to the same degree as in $\delta^{18}O$ values for quartz. Thus, while the silicon isotope ratios of minerals can exchange, the silicon isotope ratios of whole rock samples have the potential to preserve compositions obtained during BIF diagenesis even in metamorphosed BIFs. A similar conclusion for Isua rocks was also reached by André et al. (2006). Presumably, the low Si content of grain boundary metamorphic fluids contributes to small domains of exchange.

5.2. Silicon isotope fractionation processes

5.2.1. Abiotic low-temperature fractionation processes

Could abiotic processes have fractionated oxygen and silicon isotopes in the Archean and Paleoproterozoic oceans where BIFs were deposited? As noted earlier, silicon isotopes in silicic acid are fractionated on co-precipitation with Fe^{3+} hydroxides (e.g., goethite), such that ^{28}Si is preferentially partitioned and adsorbed to Fe^{3+} hydroxides ($\Delta^{30}Si(SiO_{2(adsorbed)}–H_4SiO_{4(aqueous)}) = -1.6‰$). This process gradually but only slightly increases the $\delta^{30}Si$ value of dissolved silicic acid, because of the large reservoir in the Precambrian ocean. Fractionation of silicon isotopes by adsorption of silicic acid to Fe^{3+} hydroxides was an important process in the Archean and Paleoproterozoic silicon cycle (Fischer and Knoll, 2009), and may partially explain the observed negative $\delta^{30}Si$ values of BIF quartz down to −3.7‰.

Fractionation of a similar magnitude has been inferred for precipitation of quartz from solution ($\Delta^{30}Si(SiO_{2(Qtz)}–H_4SiO_{4(aqueous)}) = -1.5‰$, Basile-Doelsch et al., 2005). A smaller fractionation was found in laboratory experiments at room temperature precipitating silica ($\Delta^{30}Si(SiO_{2(precipitated)}–H_4SiO_{4(aqueous)}) = -0.7‰$, Li et al., 1995). The largest experimental fractionation was observed with precipitated clay ($\Delta^{30}Si(clay_{(precipitated)}–clay_{(dissolved)} = -2.0‰$, Ziegler

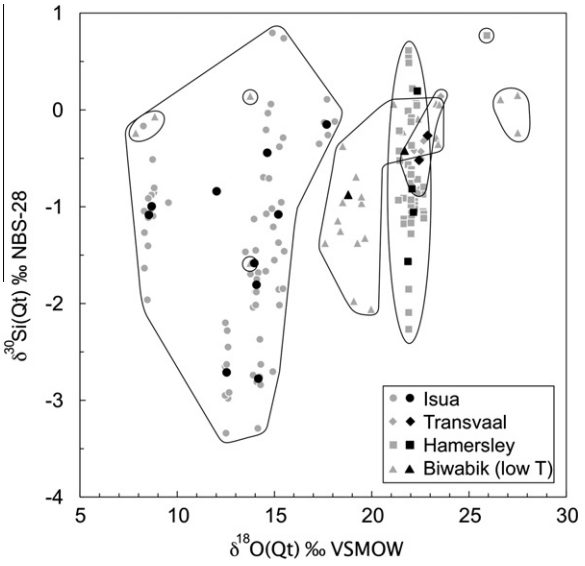

Fig. 5. Correlation of $\delta^{30}Si$ and $\delta^{18}O$ values. Bold symbols are averages for single samples, or indicate if only one correlated analysis is available. Individual analyses are gray symbols with error bars omitted for clarity (2 SD errors range from 0.2‰ to 0.4‰, see Electronic annex). Lines surround data points for each BIF locality. The average $\delta^{18}O$ values for the two low-temperature Biwabik samples exclude seven non-representative data points (see text).

et al., 2005). All of these abiotic processes fractionate the heavy isotope into solution and create lower $\delta^{30}Si$ values in the solid precipitate relative to the dissolved species. Thus, if we assume an initial fluid with mantle $\delta^{30}Si$ composition (−0.4‰; Georg et al., 2007a), the direction and magnitude of the isotope fractionations combined in sequence are sufficient to explain the range of $\delta^{30}Si$ values from mantle down to −3.7‰ measured in quartz from Isua BIFs. Additional currently unknown fractionations may have occurred, and it is also possible that fractionation factors for Si isotopes may be greater than indicated by existing experiments.

Less common values of $\delta^{30}Si$ in BIF quartz that are higher than $\delta^{30}Si$ (mantle) (Figs. 1, 3 and 4) could be caused by later precipitation from the increasingly higher $\delta^{30}Si$ residual fluids. Such a gradual increase of $\delta^{30}Si$ of fluids is consistent with precipitation in a Rayleigh distillation-like process (Valley, 1986) and is observed in precipitation experiments (Li et al., 1995; Ziegler et al., 2005; Delstanche et al., 2009). Simultaneously, there are mass-balance constraints. In a Rayleigh model, the silicon concentration of the fluid decreases due to continuous precipitation and hence the fraction of higher $\delta^{30}Si$ precipitates is much smaller compared to the earlier precipitates. This may explain the small number of higher $\delta^{30}Si$ values, as observed in Isua BIF SM-GR-99-4 (Fig. 3) but is apparently more complex for samples like Hamersley BIF 2-2-C-B where the average $\delta^{30}Si$ is above the mantle value or Isua BIF IS-622-3A where all $\delta^{30}Si$ values are $>\delta^{30}Si_{mantle}$. We will discuss below the possibility that the high $\delta^{30}Si$ values are potentially related to different sources.

5.2.2. No evidence for biological fractionation

Diatoms, radiolarians, and sponges, the silica precipitating organisms that later became important for silicon fractionation in the ocean (De La Rocha et al., 1997; De La Rocha, 2003), did not exist in the Precambrian (Kooistra and Medlin, 1996; Gehling and Rigby, 1996; Love et al., 2009). Also, land plants, which fractionate silicon isotopes during precipitation of siliceous phytoliths (Ziegler et al., 2005; Ding et al., 2005; Ding et al., 2008a,b; Opfergelt et al., 2006, 2008), did not emerge until the Ordovician (e.g., Kenrick and Crane, 1997). Laboratory experiments so far suggest that bacteria do not have an active role in silica precipitation (Yee et al., 2003; Benning et al., 2004; Lalonde et al., 2005; Amores and Warren, 2007; Phoenix and Konhauser, 2008).

The sequential combination of the abiotic fractionation effects as mentioned in the previous section could alone account for sub-mantle $\delta^{30}Si$ values in the BIF quartz, and a biologically mediated fractionation need not be invoked. The inherited $\delta^{30}Si$ microscale variability probably reflects differences in pore fluid compositions.

5.3. Sources of silicon

Some $\delta^{30}Si$ values are higher by 1‰ than mantle $\delta^{30}Si$ (Figs. 3 and 4) and as discussed above cannot be explained assuming negative $\Delta^{30}Si(Quartz\text{-}H_4SiO_4)$ and direct precipitation from hydrothermal fluids with $\delta^{30}Si$ of mantle composition (see Section 5.2.1). However, precipitation of silica from a continental source (rivers, cherts) with high $\delta^{30}Si$ would result in quartz with high $\delta^{30}Si$ values of the Proterozoic BIF samples. Van den Boorn et al. (2010) argue that the Archean ocean might have had a higher average $\delta^{30}Si$ than the modern ocean. This is in contrast to our data. In fact, we observe an average difference of about 1‰ in $\delta^{30}Si$ between Isua and the BIFs from Hamersley, Transvaal and Biwabik. Extreme negative $\delta^{30}Si$ values as measured in Isua samples would be unlikely if the ocean had a higher $\delta^{30}Si$ composition. A higher starting value of $\delta^{30}Si$ would make it virtually impossible for $\delta^{30}Si$ to reach −3.7‰, even when invoking sequential Si isotope fractionation of all described processes (see Section 5.2.1).

We conclude that continental weathering was a locally important source of silicon for the Proterozoic oceans and sometimes dominated over the hydrothermal silicon source, as reflected by the high $\delta^{30}Si$ values in Hamersley BIF sample 2-2C-B and in low temperature Biwabik BIF samples.

Hamersley sample 2-2C-B is dominantly composed of carbonate and quartz with only minor iron oxides, thus it has less Fe, thought to be hydrothermal, than oxide-rich layers in other Hamersley samples and may be closest to representing silicon values for continental input. A similar conclusion for Hamersley BIF samples was made by Hamade et al. (2003) using germanium/silicon ratios to distinguish between hydrothermal and continental silicon sources. We extend this interpretation back in time to the Eoarchean and suggest that continental runoff was locally important during deposition of the 3.8 Ga Isua BIFs. The higher than mantle $\delta^{30}Si$ values in BIF quartz could represent local continental-derived silicon. The temporal

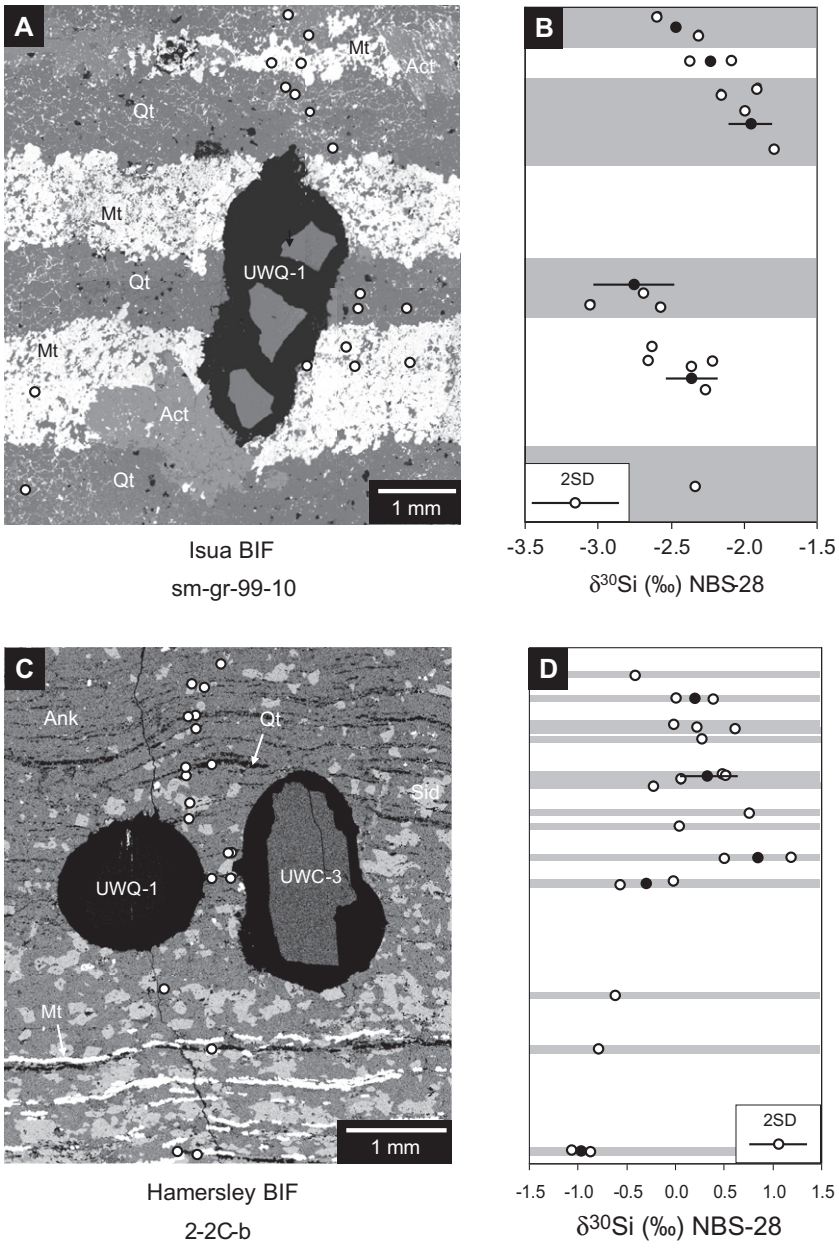

Fig. 6. BSE images of quartz and magnetite, and values of $\delta^{30}Si$(Qt) for two BIF samples. (A) BSE image of Isua sample sm-gr-99-10 containing quartz (Qt), magnetite (Mt), and actinolite (Act) along with three grains of UWQ-1 quartz standard (black is epoxy). White dots indicate placement of SIMS analysis pits. (B) Individual analyses of $\delta^{30}Si$ (white dots) and the average $\delta^{30}Si$ value (black dots) for multiple analyses in single laminae with 2 standard error (2 SE) are plotted against distance. Values of $\delta^{30}Si$ are homogeneous within $\pm 0.3‰$, the external precision at two standard deviation (2 SD) of the bracketing quartz analyses (error bar, inset), within single mm-thick laminae, but vary by up to 1.5‰ between laminae. (C) BSE image of Hamersley sample 2-2C-b containing quartz, magnetite, ankerite (Ank), and siderite (Sid) along with one grain each of UWQ-1 and UWC-3 calcite standards. White dots indicate placement of SIMS analysis pits. (D) Individual analyses of $\delta^{30}Si$ (white dots) and the average $\delta^{30}Si$ value (black dots) for multiple analyses in single laminae with 2 SE are plotted against distance. Values of $\delta^{30}Si$ are homogeneous within $\pm 0.3‰$, the external precision at two standard deviation (2 SD) of the bracketing quartz analyses (error bar, inset), within single sub-mm thick laminae, but vary by up to 2.5‰ between laminae.

variability of the two different silicon sources, hydrothermal fluids (<mantle $\delta^{30}Si$) and continental runoff (>mantle $\delta^{30}Si$), are reflected as the variability of the $\delta^{30}Si$ ratios of the analyzed BIF quartz samples in this study. If correct, these high $\delta^{30}Si$ values suggest deposition of Isua BIF in a restricted basin setting and not at a mid-ocean ridge.

6. CONCLUSIONS

1. The total range of $\delta^{30}Si$ observed in BIF quartz is 4.9‰, from −3.7‰ to 1.2‰, approximately 50% of the terrestrial $\delta^{30}Si$ range shown in Fig. 1.

2. BIF quartz samples display a large variability of $\delta^{30}Si$ on the microscale, even in highly metamorphosed samples (Isua, high-temperature Biwabik), with differences of up to 3.5‰ in a single sample (SM-GR-99-4) over distances of about a millimeter, or 1.7‰ over a distance of 80 μm (03-BIW-35E). The total range in $\delta^{30}Si$ values is not significantly different amongst variably metamorphosed BIFs. Values of $\delta^{18}O$ in individual samples from highly metamorphosed BIFs are constant presumably due to homogenization during metamorphism. Silicon isotopes are less sensitive to metamorphism than oxygen isotopes and the measured silicon isotope ratios are preserved for whole rock samples from original precursor sediments, presumably due to the lower solubility of silicon in solution. This conclusion emphasizes the importance of correlated multi-isotope *in situ* analysis at the micron-scale.
3. The most negative $\delta^{30}Si$ value (−3.7‰) of any BIF quartz was found at Isua and likely reflects hydrothermally delivered silicon that has been sequentially fractionated through adsorption onto Fe-hydroxides and later crystallization. Average $\delta^{30}Si$ values and the lowest $\delta^{30}Si$ values from Isua (3.8 Ga) are 1‰ lower than for younger (2.5–1.9 Ga) BIFs, and the $\delta^{30}Si$ values are also 1‰ lower at Isua.
4. Although quartz in Isua BIFs is dominated by low $\delta^{30}Si$ values of hydrothermal origin, higher $\delta^{30}Si$ values derived from continental weathering are also present as are values likely reflecting mixed sources. This suggests that continental weathering was a locally important process dating back to 3.8 Ga. The range of $\delta^{30}Si$ ratios in BIF quartz reflects the shifting temporal sources and relative importance of the hydrothermal and continental sources of silicon during deposition of BIFs.

ACKNOWLEDGEMENTS

We thank the following for assistance: B. Hess, sample preparation and polishing; J. Kern, SIMS and profilometer; and J. Fournelle, SEM/EDS. We thank C. M. Johnson, B. Beard, S. Moorbath, C. Klein and R. Dymek for the Isua samples; and B. Norsted for assistance in curation of Hamersley, Transvaal and Biwabik samples. We thank Associate Editor Trevor R. Ireland, two anonymous reviewers and A. Schmitt for helpful and constructive reviews, C. M. Johnson and H. Xu for helpful comments on an earlier version of the manuscript. P. R. H. was supported by the NASA Astrobiology Institute, NSF (EAR-0509639, J.W.V.), DOE (93ER14389, J.W.V.), NASA (NNX09AG39G, A. M. Davis) and the Tawani Foundation. The WiscSIMS lab is partially supported by NSF (EAR-0319230, 0744079). This research utilized NSF-supported shared facilities at the University of Wisconsin.

APPENDIX A. SUPPLEMENTARY DATA

Supplementary data associated with this article can be found, in the online version, at doi:10.1016/j.gca.2011.07.023.

REFERENCES

Amores D. R. and Warren L. A. (2007) Identifying when microbes biosilicify: the interconnected requirements of acidic pH, colloidal SiO_2 and exposed microbial surface. *Chem. Geol.* **240**, 298–312.

André L., Cardinal D., Alleman L. Y. and Moorbath S. (2006) Silicon isotopes in 3.8 Ga West Greenland rocks as clues to the Eoarchaean supracrustal silicon cycle. *Earth Planet. Sci. Lett.* **245**, 162–173.

Basile-Doelsch I., Meunier J. D. and Parron C. (2005) Another continental pool in the terrestrial silicon cycle. *Nature* **433**, 399–402.

Bau M., Hohndorf A., Dulski P. and Beukes N. J. (1997) Sources of rare-earth elements and iron in paleoproterozoic iron-formations from the Transvaal Supergroup, South Africa: evidence from neodymium isotopes. *J. Geol.* **105**(1), 121–129.

Benning L. G., Phoenix V. R., Yee N. and Tobin M. J. (2004) Molecular characterization of cyanobacterial silicification using synchrotron infrared micro-spectroscopy. *Geochim. Cosmochim. Acta* **68**, 729–741.

Bern C. R., Brzezinski M. A., Beucher C. P., Ziegler K. and Chadwick O. A. (2010) Weathering, dust, and biocycling effects on soil silicon isotope ratios. *Geochim. Cosmochim. Acta* **74**, 876–889.

Beucher C. P., Brzezinski M. A. and Jones J. L. (2008) Sources and biological fractionation of Silicon isotopes in the Eastern Equatorial Pacific. *Geochim. Cosmochim. Acta* **72**, 3063–3073.

Beukes N. J., Klein C., Kaufman A. J. and Hayes J. M. (1990) Carbonate petrography, kerogen distribution, and carbon and oxygen isotope variations in an early Proterozoic transition from limestone to iron-formation deposition, Transvaal Supergroup, South Africa. *Econ. Geol.* **85**, 663–690.

Cairns-Smith A. G. (1978) Precambrian solution photochemistry, inverse segregation, and banded iron formations. *Nature* **276**, 807–808.

Canfield D. E. (1998) A new model for Proterozoic ocean chemistry. *Nature* **396**, 450–453.

Canfield D. E. (2005) The early history of atmospheric oxygen. *Annu. Rev. Earth Planet. Sci.* **33**, 1–36.

Cardinal D., Savoye N., Trull T. W., Dehairs F., Kopczynska E. E., Fripiat F., Tison J.-L. and André L. (2007) Silicon isotopes in spring Southern Ocean diatoms: large zonal changes despite homogeneity among size fractions. *Mar. Chem.* **106**, 46–62.

Cates N. L. and Mojzsis S. J. (2007) Pre-3750 Ma supracrustal rocks from the Nuvvuagittuq supracrustal belt, northern Québec. *Earth Planet. Sci. Lett.* **255**, 9–21.

David J., Parent M., Stevenson R., Nadeau P. and Godin L. (2002) The Porpoise Cove supracrustal sequence, Inukjuak area: a unique example of Paleoarchean crust (ca. 3.8 Ga) in the Superior Province. *Ministère des Ressources Naturelles du Québec* **10**, 17.

David J., Godin L., Stevenson R., O'Neil J. and Francis D. (2009) U-Pb ages (3.8–2.7 Ga) and Nd isotope data from the newly identified Eoarchean Nuvvuagittuq supracrustal belt, Superior Craton, Canada. *GSA Bull.* **121**, 150–163.

De La Rocha C. (2003) Silicon isotope fractionation by marine sponges and the reconstruction of the silicon isotope composition of ancient deep water. *Geology* **31**, 423–426.

De La Rocha C., Brzezinski M. A. and DeNiro M. J. (1997) Fractionation of silicon isotopes by marine diatoms during biogenic silica formation. *Geochim. Cosmochim. Acta* **61**, 5051–5056.

De La Rocha C., Brzezinski M. A. and DeNiro M. J. (2000) A first look at the distribution of the stable isotopes of silicon in natural waters. *Geochim. Cosmochim. Acta* **64**, 2467–2477.

Delstanche S., Opfergelt S., Cardinal D., Elsass F., André L. and Delvaux B. (2009) Silicon isotopic fractionation during adsorption of aqueous monosilicic acid onto iron oxide. *Geochim. Cosmochim. Acta* **73**, 923–934.

Demarest M. S., Brzezinski M. A. and Beucher C. P. (2009) Fractionation of silicon isotopes during biogenic silica dissolution. *Geochim. Cosmochim. Acta* **73**, 5572–5583.

Ding T., Jiang S., Wan D., Li Y., Li J., Liu Z., Song H. and Yao X. (1996) *Silicon Isotope Geochemistry*. Geological Publishing House, Beijing, pp. 125.

Ding T., Wan D., Wang C. and Zhang F. (2004) Silicon isotope compositions of dissolved silicon and suspended matter in the Yangtze River, China. *Geochim. Cosmochim. Acta* **68**, 205–216.

Ding T. P., Ma G. R., Shui M. X., Wan D. F. and Li R. H. (2005) Silicon isotope study on rice plants from the Zhejiang province. *China. Chem. Geol.* **218**, 41–50.

Ding T. P., Zhou J. X., Wan D. F., Chen Z. Y., Wang C. Y. and Zhang F. (2008a) Silicon isotope fractionation in bamboo and its significance to the biogeochemical cycle of silicon. *Geochim. Cosmochim. Acta* **72**, 1381–1395.

Ding T. P., Tian S. H., Sun L., Wu L. H., Zhou J. X. and Chen Z. Y. (2008b) Silicon isotope fractionation between rice plants and nutrient solution and its significance to the study of the silicon cycle. *Geochim. Cosmochim. Acta* **72**, 5600–5615.

Douthitt C. B. (1982) The geochemistry of stable isotopes of silicon. *Geochim. Cosmochim. Acta* **46**, 1449–1458.

Dymek R. F. and Klein C. (1988) Chemistry, petrology and origin of banded iron-formation lithologies from the 3800 Ma Isua Supracrustal Belt, West Greenland. *Precambrian Res.* **39**, 247–302.

Ewers W. E. and Morris R. C. (1981) Studies of the Dales Gorge member of the Brockman iron formation, Western Australia. *Econ. Geol.* **76**, 1929–1953.

Ewers W. E. (1983) Chemical factors in the deposition and diagenesis of banded iron formation. In *Iron Formations: Facts and Problems* (eds. A. F. Trendall and R. C. Morris). Amsterdam, Elsevier, pp. 491–512.

Fischer W. W. and Knoll A. H. (2009) An iron shuttle for deepwater silica in late Archean and early Paleoproterozoic iron formation. *GSA Bull.* **121**, 222–235.

Fralick P., Davis D. W. and Kissin S. A. (2002) The age of the Gunflint iron formation, Ontario, Canada: single zircon U–Pb age determinations from reworked volcanic ash. *Can. J. Earth Sci.* **39**, 1085–1091.

Fripiat F., Cardinal D., Tison J.-L., Worby A. and André L. (2007) Diatom-induced silicon isotopic fractionation in Antarctic sea ice. *J. Geophys. Res.* **112**, G02001.

Garrels R. M., Perry, Jr., E. A. and Mackenzie F. T. (1973) Genesis of Precambrian iron formations and the development of atmospheric oxygen. *Econ. Geol.* **68**, 1173–1179.

Gehling J. G. and Rigby J. K. (1996) Long expected sponges from the Neoproterozoic Ediacara fauna of South Australia. *J. Paleontol.* **70**, 185–195.

Georg R. B. (2006) Geochemistry of stable silicon isotopes measured by high-resolution multi-collector inductively-coupled-plasma mass-spectrometry (HR-MC-ICP-MS). Ph. D. thesis, ETH Zurich, p. 144.

Georg R. B., Halliday A. N., Schauble E. A. and Reynolds B. C. (2007a) Silicon in the Earth's core. *Nature* **447**, 1102–1106.

Georg R. B., Reynolds B. C., West A. J., Burton K. W. and Halliday A. N. (2007b) Silicon isotope variations accompanying basalt weathering in Iceland. *Earth Planet. Sci. Lett.* **261**, 476–490.

Hamade T., Konhauser K. O., Raiswell R., Goldsmith S. and Morris R. C. (2003) Using Ge/Si ratios to decouple iron and silica fluxes in Precambrian banded iron formations. *Geology* **31**, 35–38.

Herrick M. (2007) Isotopic studies of the 3.7–3.8 Ga Isua banded iron formation provide insight into early Archean geochemical cycles. MS thesis, Univ. Wis., Madison, p. 146.

Holland H. D. (1984) *The Chemical Evolution of the Atmosphere and Oceans*. Princeton Univ. Press, Princeton, New Jersey, 582 pp.

Jiang S. Y., Ding T. P., Wan D. F. and Li Y. H. (1993) Silicon isotopic compositions of Archean banded Si-Fe formation (BIF) in the Gongchangling Ore deposit, Liaoning Province, China. *Sci. China (Series B)* **36**, 482–489.

Johnson C. M., Beard B. L., Beukes N. J., Klein C. and O'Leary J. M. (2003) Ancient geochemical cycling in the Earth as inferred from Fe isotope studies of banded iron formations from the Transvaal Craton. *Contrib. Mineral. Petrol.* **144**, 523–547.

Johnson C. M., Beard B. L., Klein C., Beukes N. J. and Roden E. E. (2008) Iron isotopes constrain biologic and abiologic processes in banded iron formation genesis. *Geochim. Cosmochim. Acta* **72**, 151–169.

Jones L. H. P. and Handreck K. A. (1963) Effects of iron and aluminium oxides on silica in solution in soils. *Nature* **198**, 852–853.

Kaufmann A. J. (1996) Geochemical and mineralogic effects of contact metamorphism on banded iron-formation: an example from the Transvaal Basin, South Africa. *Precambrian Res.* **79**, 171–194.

Kelly J. L., Fu B., Kita N. T. and Valley J. W. (2007) Optically continuous silcrete quartz cements of the St. Peter Sandstone: high precision oxygen isotope analysis by ion microprobe. *Geochim. Cosmochim. Acta* **71**, 3812–3832.

Kenrick P. and Crane P. R. (1997) The origin and early evolution of plants on land. *Nature* **389**, 33–39.

Kirschvink J. L. (1992) Late Proterozoic low-latitude global glaciation: the snowball Earth. In *The Proterozoic Biosphere* (eds. J. W. Schopf and C. Klein). Cambridge Univ. Press. pp. 51–52.

Kita N. T., Ushikubo T., Fu B. and Valley J. W. (2009) High precision SIMS oxygen isotope analyses and the effect of sample topography. *Chem. Geol.* **264**, 43–57.

Klein C. and Beukes N. J. (1989) Geochemistry and sedimentology of a facies transition from limestone to iron-formation deposition in the Early ProterozoicTransvaal Supergroup, South Africa. *Econ. Geol.* **84**, 1733–1774.

Knight K. B., Kita N. T., Mendybaev R. A., Richter F. M., Davis A. M. and Valley J. W. (2009) Silicon isotopic fractionation of CAI-like vacuum evaporation residues. *Geochim. Cosmochim. Acta* **73**, 6390–6401.

Kooistra W. H. C. F. and Medlin L. K. (1996) Evolution of the Diatoms (Bacillariophyta). IV. A reconstruction of their age from small subunit rRNA coding regions and the fossil record. *Mol. Phylogenet. Evol.* **6**, 391–407.

Lalonde S. V., Konhauser K. O., Reysenbach A.-L. and Ferris F. G. (2005) Thermophilic silicification: the role of *Aquificales* in hot spring sinter formation. *Geobiology* **3**, 41–52.

Lepp H. and Goldich S. S. (1964) Origin of Precambrian iron formations. *Econom. Geol.* **59**, 1025–1060.

Li Y. H., Ding T. P. and Wan D. F. (1995) Experimental study of silicon isotope dynamic fractionation and its application in geology. *Chinese J. Geochem.* **14**, 212–219.

Love G. D., Grosjean E., Stalvies C., Fike D. A., Grotzinger J. P., Bradley A. S., Kelly A. E., Bhatia M., Meredith W., Snape C. E., Bowring S. A., Condon D. J. and Summons R. E. (2009) Fossil steroids record the appearance of Demospongiae during the Cryogenian period. *Nature* **457**, 718–722.

Lovley D. R., Stolz J. F., Nord G. L. and Phillips E. J. P. (1987) Anaerobic production of magnetite by a dissimilatory iron-reducing microorganism. *Nature* **330**, 252–254.

Marin J., Chaussidon M. and Robert F. (2010) Microscale oxygen isotope variations in 1.9 Ga Gunflint cherts: assessments of

diagenesis effects and implications for oceanic paleotemperature reconstructions. *Geochim. Cosmochim. Acta* **74**, 116–130.

Milligan A. J., Varela D. E., Brzezinski M. A. and Morel F. M. M. (2004) Dynamics of silicon metabolism and silicon isotopic discrimination in a marine diatom as a function of pCO_2. *Limnol. Oceanogr.* **49**, 322–329.

Molini-Velsko C., Mayeda T. K. and Clayton R. N. (1986) Isotopic composition of silicon in meteorites. *Geochim. Cosmochim. Acta* **50**, 2716–2719.

Moorbath S., O'Nions R. K., Pankhurst R. J. and McGregor V. R. (1973) Early Archean age for the Isua iron formation, West Greenland. *Nature* **245**, 138–139.

Morris R. C. (1993) Genetic modeling for banded iron formation of the Hamersley Group, Pilbara Craton, Western Australia. *Precambrian Res.* **60**, 243–286.

Opfergelt S., Cardinal D., Henriet C., André L. and Delvaux B. (2006) Silicon isotope fractionation between plant parts in banana: in situ vs. in vitro. *J. Geochem. Explor.* **88**, 224–227.

Opfergelt S., Delvaux B., André L. and Cardinal D. (2008) Plant silicon isotopic signature might reflect soil weathering degree. *Biogeochemistry* **91**, 163–175.

Phoenix V. R. and Konhauser K. O. (2008) Benefits of bacterial biomineralization. *Geobiology* **6**, 303–308.

Robert F. and Chaussidon M. (2006) A paleotemperature curve for the Precambrian oceans based on silicon isotopes in cherts. *Nature* **443**, 969–972.

Siever R. (1992) The silica cycle in the Precambrian. *Geochim. Cosmochim. Acta* **56**, 3265–3272.

Steinhoefel G., Horn I. and von Blanckenburg F. (2009) Micro-scale tracing of Fe and silicon isotope signatures in banded iron formation using femtosecond laser ablation. *Geochim. Cosmochim. Acta* **73**, 5342–5360.

Steinhoefel G., von Blanckenburg F., Horn I., Konhauser K. O., Beukes N. J. and Gutzmer J. (2010) Deciphering formation processes of banded iron formations from the Transvaal and the Hamersley successions by combined Si and Fe isotope analysis using UV femtosecond laser ablation. *Geochim. Cosmochim. Acta* **74**, 2677–2696.

Sumner D. Y. (1997) Carbonate precipitation and oxygen stratification in Late Archean seawater as deduced from facies and stratigraphy of the Gamohaan and Frisco Formations, Transvaal Supergroup, South Africa. *Am. J. Sci.* **297**, 455–487.

Sumner D. Y. and Bowring S. A. (1996) U–Pb geochronologic constraints on deposition of the Campbellrand Subgroup, Transvaal Supergroup, South Africa. *Precambrian Res.* **79**, 29–35.

Trendall A. F. and Blockley J. G. (1970) The iron formations of the Precambrian Hamersley Group, Western Australia, with special reference to the associated crocidolite. *W. Aust. Geol. Surv. Bull.* **110**, 365 pp.

Trendall A. F., Compston W., Williams I. S., Armstrong R. A., Arndt N. T., McNaughton N. J., Nelson D. R., Barley M. E., Beukes N. J., de Laeter J. R., Retief E. A. and Thorne A. M. (1990) Precise zircon U–Pb chronological comparison of the volcano-sedimentary sequences of the Kaapvaal and Pilbara cratons between about 3.1 and 2.4 Ha. In (compilers) *Third International Archean Symposium Extended Abstracts Volume* (eds. J. E. Glover and J. E. Jo). Geoconferences (W.A.) Inc., Perth. pp. 81–83.

Trendall A. F., Compston W., Nelson D. R., De Laeter J. R. and Bennett V. C. (2004) SHRIMP zircon ages constraining the depositional chronology of the Hamersley Group, Western Australia. *Aust. J. Earth Sci.* **51**, 621–644.

Valaas Hyslop E., Valley J. W., Johnson C. M. and Beard B. L. (2008) The effects of metamorphism on O and Fe isotope compositions in the Biwabik iron formation, northern Minnesota. *Contrib. Mineral. Petrol.* **155**, 313–328.

Valley J. W. (1986) Stable isotope geochemistry of metamorphic rocks. *Rev. Mineral.* **16**, 445–489.

Valley J. W. (2001) Stable isotope thermometry at high temperatures. *Rev. Mineral. Geochem.* **43**, 365–414.

Valley J. W and Kita N. T. (2009) *In situ* oxygen isotope geochemistry by ion microprobe. In *Secondary Ion Mass Spectrometry in the Earth Sciences: Gleaning the Big Picture from a Small Spot*, vol. 41 (ed. M. Fayek). Mineral. Assoc. Canada Short Course Series. pp. 19–63.

Van den Boorn S. H. J. M., van Bergen M. J., Nijman W. and Vroon P. Z. (2007) Dual role of seawater and hydrothermal fluids in Early Archean chert formation: evidence from silicon isotopes. *Geology* **35**, 939–942.

Van den Boorn S. H. J. M., van Bergen M. J., Vroon P. Z., de Vries S. T. and Nijman W. (2010) Silicon isotope and trace element constraints on the origin of 3.5 Ga cherts: implications for Early Archean marine environments. *Geochim. Cosmochim. Acta* **74**, 1077–1103.

Wu S. Y., Zhang D. J., Wang K. Y., Chen C. Y. and Bai L. M. (2000) Geochemical characteristics of stable isotopes from hydrothermal chimneys in the Mariana trough, West Pacific Ocean. *Chinese J. Oceanol. Limnol.* **18**, 378–384.

Yee N., Phoenix V. R., Konhauser K. O., Benning L. G. and Ferris F. G. (2003) The effect of cyanobacteria on silica precipitation at neutral pH: implications for bacterial silicification in geothermal hot springs. *Chem. Geol.* **199**, 83–90.

Ziegler K., Chadwick O. A., Brzezinski M. A. and Kelly E. F. (2005) Natural variations of $\delta^{30}Si$ ratios during progressive basalt weathering, Hawaiian Islands. *Geochim. Cosmochim. Acta* **69**, 4597–4610.

Associate editor: Trevor Ireland